Why p-OMe- and p-Cl-beta-Methylphenethylamines Display Distinct Activities uponMAO-B Binding

Angélica Fierro, *Pontificia Universidad Católica de Chile*
Dale Edmondson, *Emory University*
Cristian Celis-Barros, *Universidad Andres Bello*
Marco Rebolledo-Fuentes, *University of Chile*
Gerald Zapata-Torres, *University of Chile*

Final published version: http://dx.doi.org/10.1371/journal.pone.0154989
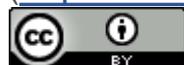
Accessed November 25, 2020 9:01 PM EST

RESEARCH ARTICLE

Why p-OMe- and p-Cl-β-Methylphenethylamines Display Distinct Activities upon MAO-B Binding

Angélica Fierro[1]ↀ, Dale E. Edmondson[2]ↀ, Cristian Celis-Barros[3]*, Marco Rebolledo-Fuentes[4]ↀ, Gerald Zapata-Torres[5]*

1 Facultad de Química, Departamento de Química Orgánica, Pontificia Universidad Católica de Chile, Santiago, Chile, 2 Departments of Chemistry and Biochemistry, Emory University, Atlanta, GA, United States of America, 3 Universidad Andres Bello, Facultad de Ciencias Exactas, Departamento de Ciencias Quimicas, Santiago, Chile, 4 Department of Chemistry, Faculty of Sciences, University of Chile, Santiago, Chile, 5 Faculty of Chemical and Pharmaceutical Sciences, University of Chile, Santiago, Chile

ↀ These authors contributed equally to this work.
* gzapata@uchile.cl

Abstract

Despite their structural and chemical commonalities, p-chloro-β-methylphenethylamine and p-methoxy-β-methylphenethylamine display distinct inhibitory and substrate activities upon MAO-B binding. Density Functional Theory (DFT) quantum chemical calculations reveal that β-methylation and para-substitution underpin the observed activities sustained by calculated transition state energy barriers, attained conformations and key differences in their interactions in the enzyme's substrate binding site. Although both compounds meet substrate requirements, it is clear that β-methylation along with the physicochemical features of the para-substituents on the aromatic ring determine the activity of these compounds upon binding to the MAO B-isoform. While data for a larger set of compounds might lend generality to our conclusions, our experimental and theoretical results strongly suggest that the contrasting activities displayed depend on the conformations adopted by these compounds when they bind to the enzyme.

Introduction

The biogenic amine levels in human cells are controlled in part by their oxidation by ubiquitous enzymes known as monoamine oxidases (MAOs). Since the discovery of the antidepressant activities of certain molecules acting as MAO inhibitors (MAOi) around 1950 [1], these enzymes have been associated with neurological and neurodegenerative pathologies such as depression, Parkinson's and Alzheimer's diseases [2]. These enzymes, inserted in the outer membrane of mitochondria, use flavin adenine dinucleotide (FAD) as a cofactor [3]. Even though the clinically most relevant endogenous substrates of MAOs are serotonin (5-HT) and dopamine (DA), these enzymes are able to oxidize other monoamines such as benzylamine (BA), phenylethylamine (PEA) and their derivatives [4–8]. Human MAO exists in two isoforms, known as A and B, sharing ca. 70% of sequence identity. Although several MAO crystal structures are available [9–22], the mechanisms of selectivity regarding substrates and inhibitors for each isoform have not yet reached a consensus. New insights regarding the possible

catalytic mechanisms for the oxidative deamination of neurotransmitter amines by mono-amine oxidase B have recently become available [23–26]. Earlier investigations focused largely on the active site of MAOs, located in a cavity lined mainly by hydrophobic residues [27, 28]. A special sector of this active site consists of the so-called "aromatic cage" which contains the FAD cofactor and two tyrosine residues with their rings perpendicular to the isoalloxazine moiety of FAD. It is known that many MAO substrates become inhibitors when they are α-methylated, and most of these products inhibit MAO-A selectively. In contrast, β-methylation of MAO substrates often generates selective MAO-B inhibitors [29]. Almost 30 years ago, Kinemuchi et al. [30] studied 5-fluoro-α-methyltryptamine (5-FMT) and p-chloro-β-methyl-phenethylamine (p-CMP). These authors found that both molecules act as selective and revers-ible inhibitors of MAO-A and MAO-B, respectively. Later results by Kim et al. [31] confirmed that p-CMP was a short-acting, probably reversible, MAO-B selective inhibitor. In this article, we report the interesting change in the biological activity displayed by a couple of β-methylphe-nylalkylamines, where the inhibitor p-CMP becomes a substrate when a methoxyl group replaces its para-chloro substituent.

Materials and Methods

Biological evaluation

MAO-B was expressed in *Pichia pastoris* and purified as described previously by Newton-Vin-son *et al.* [32] The final step in the preparation of MAO-B used 50 mM potassium phosphate buffer pH 7.4, 50% glycerol, and 0.8% n-octyl-β-d-glucopyranoside (w/v). MAO activity assays were performed by monitoring the rate of product formation over time at 25°C using a Perkin-Elmer Lambda 2 spectrophotometer. p-Methoxy-β-methylphenethylamine oxidation was monitored spectrometrically using the horseradish peroxidase-coupled Amplex Red assay ($\Delta\varepsilon = 54\,000$ M^{-1}•cm^{-1}, $\lambda = 560$ nm). A similar experiment was carried out with kynuramine ($\Delta\varepsilon = 12\,000$ M^{-1}•cm^{-1}, $\lambda = 316$ nm) to obtain a control value by monitoring its oxidation.

General methods

^{1}H and ^{13}C NMR spectra were recorded on a Bruker Avance 500 MHz spectrometer at 300 K. Coupling constants in Hz were measured from-one dimensional spectra. HRMS-ESI analyses were carried out using a Thermo Scientific Exactive Plus Orbitrap spectrometer with a constant nebulizer temperature of 250°C. The experiment was carried out in positive ion mode at high resolution (resolving power: 140,000 (full width half-maximum peak width at m/z 300, R$_{fwhm}$). The samples were infused directly into the ESI source using a syringe pump at flow rates of 5 μL min^{-1}. All chemicals were reagent grade and used without further purification (S1 Fig).

2-(4-Methoxyphenyl)propan-1-aminium chloride. 1 g (0,006 mol) of 4-methoxynitros-tyrene was dissolved in 50 mL of dry tetrahydrofuran (THF). To this solution, a mixture of 6 mL of a 3 M solution of methylmagnesium bromide (CH$_3$MgBr) in diethyl ether was added (3:1 ratio), stirring overnight at room temperature. Silica gel column and thin layer chromatog-raphy (9:1 ethanol:methanol) were used to purify the main product. Once separated, the sol-vent was removed using a rotary evaporator and the product weighed. This intermediate, dissolved in dry THF, was slowly added to a suspension of lithium aluminium hydride (LiAlH$_4$; 1:1 in mass), and the mixture was refluxed overnight. Once the reduction was com-plete, drops of saturated aqueous sodium hydroxide (NaOH) and isopropyl alcohol (IPA) were added to form a solid cake that was then washed with THF and filtered. The solvent (mainly THF) fraction was concentrated as before, and the amine residue was distilled (190°C at 10 Torr). The distilled product was neutralized using a saturated solution of hydrochloric acid in methanol to obtain a white solid (43% overall yield). ^{1}H NMR (400 MHz, MeOH-d$_4$) δ 7.25 (d,

J = 8.4 Hz, 2H), 6.95 (d, J = 8.4 Hz, 2H), 3.80 (s, 3H), 3.162 (m, 2H), 3.02 (m, 1H), 1.34 (d, J = 6.4 Hz, 3H). ^{13}C NMR (125 Hz, MeOH-d$_4$, 300 K): δ 159.13, 133.54, 127.89, 114.15 (ArC), δ 54.37 (OCH$_3$), δ 47.63 (CH$_2$NH$_2$), δ 37.36 (CH), δ 18.64 (CH$_3$) ppm. HRMS for C$_{10}$H$_{16}$NO [M-Cl]$^+$ m/z Calcd: 166.1226. Observed: 166.1223 (S2 Fig).

Theoretical calculations

To obtain structural and energetic information regarding the MAO-B/p-CMP and MAO-B/p-MMP complexes, we applied the quantum chemical cluster approach for modeling enzyme reactions. This methodology considers a selected part of the enzyme (ca. 229 atoms for p-CMP, 233 atoms for p-MMP) provided that this small cluster behaves like the real system (S3 and S4 Figs), taking into account two the steric constraints imposed by the enzyme on the active site and long-range polarization effects. Steric constraints consider all the side chain Cαs of the cluster residues for MAO-B as locked into their crystallographic positions. Long range polarization effects take into account solvation effects using the CPCM conductor-like polarizable continuum model [33,34] with two dielectric constants, i.e. ε = 4 and ε = 80, performing single-point calculations on the optimized structures. The strength of this methodology makes the cluster selection independent of the dielectric constant [35]. Cluster selection was carried out using the crystal structure of human MAO-B expressed in *Pichia pastoris* complexed with p-nitrobenzylamine (NBA) (PDB code 2C70) [22]. NBA is bound to the binding site with its side chain pointing towards the FAD cofactor. Since no crystal structures are available for p-CMP and p-MMP, the pose adopted by NBA was used to locate their aromatic moieties. The active site models included the isoalloxazine ring, Tyr398 and Tyr435, Tyr188, Gln206, Lys296, Cys172, Ile199 and Tyr326 and six water molecules present in this crystal structure, further verified by the WaterDock [36] script in the Vina Docking program.

All calculations were carried out using the meta-hybrid GGA functional M06-2X [37] implemented in the Gaussian09 suite of programs [38]. Geometries were optimized using the 6-31G(d,p) basis set. In order to get more accurate energies, single-point calculations were carried out on the optimized geometries using the larger 6–311+G(2d,2p) basis set. Frequencies were computed analytically at the same level of theory as the geometry optimizations to confirm whether the obtained structures were minima or transition states and to obtain zero-point energy (ZPE) corrections. The final reported energies consist of the large basis set energies corrected for ZPE, solvation, and dispersion effects. In order to unequivocally assign reactants and products we scaled the transition state frequencies, which then were optimized and confirmed as local minima. Imaginary frequencies of the enzymatic transition states were -1153.3, and -1048.8 cm^{-1} for p-CMP and p-MMP, respectively.

The reaction rate constant (k) can be expressed as:

$$k = \frac{k_b T}{h} e^{\frac{-\Delta G^{\neq}}{RT}}$$

(1)

For enzymatic reactions, the calculated reaction barrier can be compared with the experimental kinetic results, provided k_{cat} is available. Thus, the experimental Gibbs free energy barrier was obtained from kinetic rate constants using Eq 2.

$$\Delta G^{\neq}_{exp} = -RT \ln\left(\frac{kh}{k_b T}\right)$$

(2)

where k = rate constant; k_b = Boltzmann constant; T = temperature; $\Delta G^{\neq}$ = free energy of activation; h = Planck's constant; R = gas constant. This equation is valid for simple transition state theory where the transmission coefficient is approximated to unity [39].

NCIPLOT software was used to understand the anchoring of the studied compounds at the active site. This program calculates the NCI indexes, which are based on the reduced density gradient defined as s(ρ) ([Eq 3](#)) at low densities and accounting for non-covalent interactions such as van der Waals, steric clashes and hydrogen bonds.

$$s = \frac{1}{2(3\pi^2)^{1/3}} \frac{\nabla\rho}{\rho^{4/3}} \tag{3}$$

In order to recognize the nature of the non-bonded interactions, the sign of the second eigenvalue (λ2) of the Laplacian of the density is related to: 1) hydrogen bonds if λ2 < 0, 2) steric repulsion if λ2 > 0 and 3) van der Waals interactions if λ2 ≈ 0. Therefore, ρ*sign(λ2) ranges from negative to positive values and the density itself is used to evaluate the strength of the interaction [40,41]. Analysis of NCI peaks is needed to differentiate between interaction types. The sign of the Laplacian of the density ($\nabla^2\rho$) indicates whether the net gradient flux is entering ($\nabla^2\rho < 0$) or leaving ($\nabla^2\rho > 0$) an infinitesimal volume around a reference point. Hence, it highlights whether the density is concentrated or depleted at that point, relative to the surrounding environment [42].

Results and Discussion

In order to study the influence of the para-substituent on the activity of β-methylphenylalkylamines, we prepared p-methoxy-β-methylphenethylamine (p-MMP) where the chlorine atom is replaced by a sterically similar methoxyl group on the aromatic ring. As mentioned before, Kinemuchi et al. and Kim et al. [30, 31] found that p-CMP was a highly selective MAO-B-inhibitor. However, we found that its p-methoxyl counterpart behaves like a selective substrate, with a low k_{cat} of 14 min^{-1} and a Michaelis constant of 87 μM compared to phenylethylamine (PEA) which is described as a good MAO-B substrate (K_{cat} 300 min^{-1} and K_m 0.016 mM) [21]. According to these experimental results, we hypothesize that the nature of the *para*-substituent determines the agonist or antagonist character displayed by these substrate analogues with MAO-B. [Table 1](#) shows that p-chlorophenethylamine (p-CP), as a model of compounds lacking the β-methyl group, is a poor substrate with a K_{cat} of 3.41 min^{-1}, and β-methylation (as in the case of p-CMP) turns this molecule into an inhibitor (K_i = 0.55 μM) as reported by Kinemuchi et al. [30]

We modelled the rate-determining step and calculated the reactant, transition state and product energies and free Gibbs energy barriers for the MAO-B/p-CMP and MAO-B/p-MMP complexes ([S1 Table](#)). All states were confirmed as ground or transition states according to their calculated frequencies. Our results show that the p-chloro derivative displays a higher activation energy compared to its p-methoxylated counterpart (35 kcal/mol vs 19.5 kcal/mol).

Table 1. p-CMP and p-MMP kinetic constants for MAO-B and experimental and calculated free Gibbs energy barriers.

Molecule	K_i (μM)	k_{cat} (min^{-1})	K_m (μM)	$\Delta G^{\ddagger}{}_{exp}$[e] (kcal/mol)	$\Delta G^{\ddagger}{}_{theo}$[e] (kcal/mol)
PEA	N.D.	228 ± 0.9[a]	16 ± 1[a]	16.7[b]	17.1[b]
p-CP[c]	N.D.	3.41 ± 0.12	2.4 ± 0.2	19.15	N.C.
p-CMP	0.55[d]	N.D.	N.D.	N.D.	35.0
p-MMP	N.D.	14 ± 1	87 ± 8	18.3	19.5

[a] Constants reported by Li et al. [21].

[b] Constants reported by Zapata et al. [23].

[c] Constants reported by Heuson et al. [43].

[d] Constants reported by Kinemuchi et al. [30].

[e] See Electronic Supplementary Information. N.D. = Not Determined. N.C. = Not Calculated.

doi:10.1371/journal.pone.0154989.t001

The lower energy barrier displayed by p-MMP is in agreement with the obtained experimental value of 18.3 kcal/mol (Table 1). It is worth mentioning that energy barriers higher than 25 kcal/mol make enzyme catalysis very unlikely [44]. Also, NCI (non-covalent interaction) indexes were evaluated to provide information regarding weak ligand-enzyme interactions based on the reduced density gradient in low-density regions [40–42]. These interactions are important since they govern, not only the anchorage, but also the stabilization of the substrate orientations at the binding site. Inspection of the obtained TS geometries of both complexes (Fig 1) shows that the bound p-CMP ring is rotated by ca. 60° with respect to that of p-MMP.

This conformation is best explained by the non-covalent interactions established in the active site by p-CMP. Also, taking into account the anisotropic electronic distribution on the chlorine atom [45], the generation of a positive σ hole at the far end of the C-Cl bond allows a specific and orthogonal hydrogen bond to form. Specifically, a weak hydrogen bond can be seen between the chlorine atom of p-CMP and the amide moiety of Cys172 (S5 Fig). Fig 1 shows that the prevailing interactions for p-CMP are van der Waals in nature according to the NCI indexes (light green coloured).

On the other hand, the methoxyl oxygen atom of p-MMP also interacts with the thiol hydrogen of Cys172; however, its methyl group is located opposite to the position of the chloride atom of p-CMP (Fig 1B and 1D, and S6 Fig).

The differences described above are directly related to the interactions established in the reactive region of the TS structures, which comprises N5 and C4a of FAD, and the amine nitrogen (Nam), Cα and Hα of the substrate (Fig 2). In Fig 1A and 1C it can be seen that p-MMP displays stronger interactions than p-CMP. Specifically, p-MMP exhibits a strong hydrogen bond between O4 of FAD and a conserved water molecule linking FAD to Lys296.

This water molecule has been reported to be important in catalysis, stabilising the TS by linking Lys296 to FAD [23]. Additionally, we note that both p-CMP and p-MMP display an interaction between Nam and C4a of the flavin, which has been suggested to occur in the polar nucleophilic mechanism (S7 Fig) [23]. Also, it should be emphasized that the TS of p-MMP is stabilized by a strong hydrogen bonding network of water molecules, which in the case of p-CMP is almost absent (Fig 3). This loss of hydrogen bonding interactions explains the calculated difference in the activation energies of both molecules (ca. 15 kcal/mol).

Our findings indicate that β-methyl substitution on phenethylamines allows substrates to adopt a suitable orientation to undergo catalysis; i.e. leaving the pro-R Hα pointing towards N5 of FAD. However, the other interactions established only by p-MMP allow the proper orientation of its aromatic ring parallel to the two tyrosine residues of the aromatic cage, thus mimicking other MAO-B substrates [23]. Therefore, conformational constraints imposed by β-methylation in combination with the restricted interaction displayed by the p-chlorine substituent and the breaking of the water network place p-CMP in the substrate pocket but with features that do not allow the oxidation to occur. These results are in agreement with previous conclusions of Edmondson et al. [46] who argue that the para-position of the bound substrate is in a hydrophobic domain of limited size. With these restrictions, bound p-MMP can adopt an orientation that favors its substrate character.

Conclusions

In conclusion, although both p-CMP and p-MMP meet the structural requirements for MAO-B substrates, it is clear that the combined presence of a β-methyl group and para-substituents of similar volume but different electronic properties on the aromatic ring, determines the agonist or antagonist activity of these compounds. While experimental data for a larger set of compounds would most likely enrich this discussion, our experimental and theoretical results
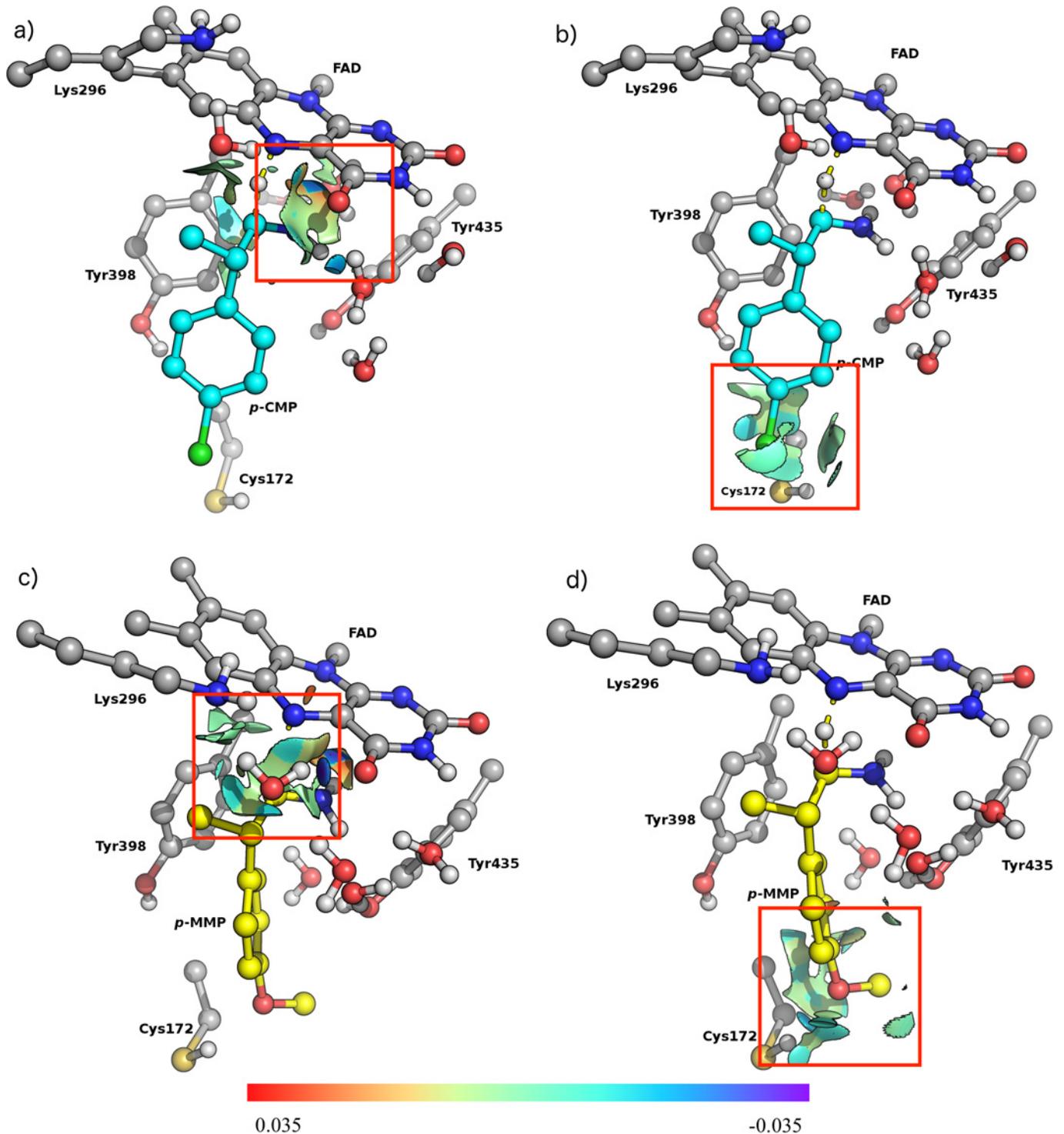
Fig 1. Non-covalent interaction (NCI) surface for binding site models in TS complexes with p-CMP and p-MMP after QM optimization. Red squares indicate hydrogen bonds (blue surfaces) and favorable van der Waals interactions (light green surfaces). a) the reactive region of p-CMP; b) p-substituent region of p-CMP, c) the reactive region of p-MMP and d) p-substituent region of p-MMP. p-CMP is depicted in cyan ball and sticks while p-MMP is depicted in yellow ball and sticks. NCI indexes isovalues range from 0.035 to -0.035 (au). p-MMP (p-methoxy-β-methylphenylethylamine); p-CMP (p-chloro-β-mehtylphenylethylamine), respectively.
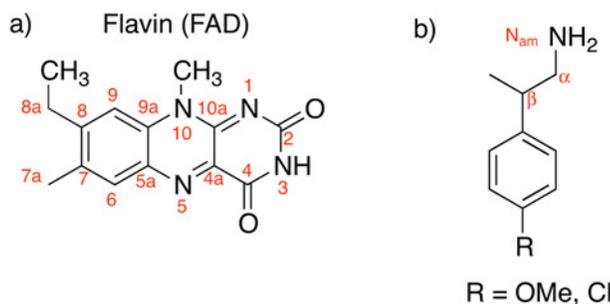
doi:10.1371/journal.pone.0154989.g001

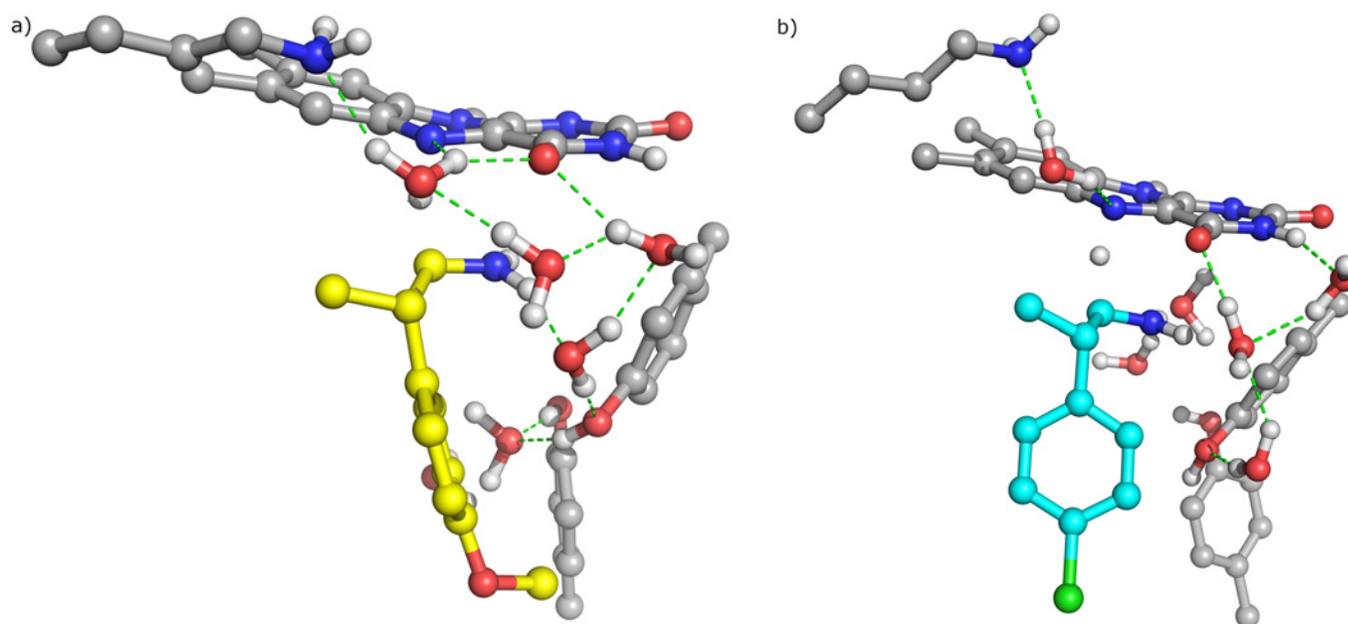Fig 2. Structure and nomenclature. a) isoalloxazine ring of FAD. b) p-CMP or p-MMP.

Fig 3. Hydrogen bond network. In a) p-CMP and b) p-MMP at the active site of MAO-B.

strongly suggest that the different activities displayed by these two very similar compounds depends on the conformation they can adopt upon binding in the MAO-B catalytic site.

Supporting Information

S1 Fig. HRMS-ESI spectrum. HRMS-ESI analyses were carried out by using a Thermo Scientific Exactive Plus Orbitrap spectrometer with a constant nebulizer temperature of 250° C. The experiment was carried out in positive ion mode at high resolution (resolving power: 140,000 (full width half-maximum peak width at m/z 300, R_{fwhm}). The samples were infused directly into the ESI source using a syringe pump at flow rates of 5 μL min^{-1}.
(PDF)

S2 Fig. Plots of ^{1}H and ^{13}C NMR spectra.
(PDF)

S3 Fig. Cluster considered for the transition state structure for p-CMP. Atoms and bonds are depicted as balls and sticks. p-CMP in cyan. All other atoms are depicted as follows: carbon

atoms in grey, oxygen atoms in red, nitrogen atoms in blue and hydrogen atoms in white.
(PDF)

S4 Fig. Cluster considered for the transition state structure for p-MMP. Atoms and bonds are depicted as balls and sticks. p-MMP in yellow. All other atoms are depicted as follows: carbon atoms in grey, oxygen atoms in red, nitrogen atoms in blue and hydrogen atoms in white.
(PDF)

S5 Fig. Full NCI indexes of the transition state of p-CMP at the active site. NCI indexes coloured ranging from 0.035 to -0.035 (au). For the sake of clarity some amino acid side-chains have been deleted from the figure.
(PDF)

S6 Fig. Full NCI indexes of the transition state of p-MMP at the active site. NCI indexes iso-values coloured ranging from 0.035 to -0.035 (au). For the sake of clarity some amino acid side-chains have been deleted from the figure.
(PDF)

S7 Fig. Proposed polar nucleophilic mechanism. This mechanism involves a proton transfer by means of a Nam-C4a adduct.
(PDF)

S1 Table. Calculated contributions to free energy of activation for p-CMP and p-MMP complexed with MAO-B.
(PDF)

Author Contributions

Conceived and designed the experiments: AF DEE CCB MRF GZT. Performed the experiments: AF DEE CCB MRF GZT. Analyzed the data: AF DEE CCB MRF GZT. Contributed reagents/materials/analysis tools: AF DEE CCB MRF GZT. Wrote the paper: AF DEE CCB MRF GZT. DFT Calculations and analysis of results: GZT CCB. Synthesis: MRF. Kinetic constants measurements for MAO-B: AF DEE.

References

1. Pletscher A. The discovery of antidepressants: a winding path. Experientia. 1991; 47: 4–8. PMID: 1999242

2. Song MS, Matveychuk D, MacKenzie EM, Duchcherer M, Mousseau DD, Baker GB. An update on amine oxidase inhibitors: multifaceted drugs. Prog Neuropsychopharmacol Biol Psychiatry. 2013; 44: 118–24. doi: 10.1016/j.pnpbp.2013.02.001 PMID: 23410524

3. Youdim MB, Edmondson D, Tipton KF. The therapeutic potential of monoamine oxidase inhibitors. Nat Rev Neurosci. 2006; 7: 295–309. PMID: 16552415

4. Edmondson DE, Binda C, Wang J, Upadhyay AK, Mattevi A. Molecular and mechanistic properties of the membrane-bound mitochondrial monoamine oxidases. Biochemistry. 2009; 48: 4220–4230. doi: 10.1021/bi900413g PMID: 19371079

5. Miller JR, Edmondson DE. Structure-activity relationships in the oxidation of para-substituted benzyla-mine analogues by recombinant human liver monoamine oxidase A. Biochemistry. 1999; 38: 13670–13683. PMID: 10521274

6. Walker MC, Edmondson DE. Structure-activity relationships in the oxidation of benzylamine analogs by bovine liver mitochondrial monoamine oxidase B. Biochemistry. 1994; 33: 7088–7098. PMID: 8003474

7. Nandigama RK, Edmondson DE. Structure-activity relations in the oxidation of phenethylamine analogues by recombinant human liver monoamine oxidase A. Biochemistry. 2000; 39: 15258–15265. PMID: 11106506

8. Yang HYT, Neff NH. β-Phenylethylamine: a specific substrate for type B monoamine oxidase of brain. J Pharmacol Exp Ther. 1973; 187: 365–371. PMID: 4748552

9. De Colibus L, Li M, Binda C, Lustig A, Edmondson DE, Mattevi A. Three-dimensional structure of human monoamine oxidase A (MAO-A): relation to the structures of rat MAO A and human MAO-B. Proc Natl Acad Sci USA. 2005; 102: 12684–12689. PMID: 16129825

10. Milczek EM, Bonivento D, Binda C, Mattevi A, McDonald IA, Edmondson DE. Structural and Mechanistic Studies of Mofegiline Inhibition of Recombinant Human Monoamine Oxidase B. J Med Chem. 2008; 51: 8019–8026. doi: 10.1021/jm8011867 PMID: 19053775

11. Binda C, Hubálek F, Li M, Herzig Y, Sterling J, Edmondson DE, et al. Binding of rasagiline-related inhibitors to human monoamine oxidases: a kinetic and crystallographic analysis. J Med Chem. 2005; 48: 8148–8154. PMID: 16366596

12. Binda C, Wang J, Li M, Hubálek F, Mattevi A, Edmondson DE. Structural and Mechanistic Studies of Arylalkylhydrazine Inhibition of Human Monoamine Oxidases A and B. Biochemistry. 2008; 47: 5616–5625. doi: 10.1021/bi8002814 PMID: 18426226

13. Binda C, Aldeco M, Geldenhuys WJ, Tortorici M, Mattevi A, Edmondson DE. Molecular insights into human monoamine oxidase B inhibition by the glitazone antidiabetes drugs. ACS Med Chem Lett. 2011; 3: 39–42. PMID: 22282722

14. Binda C, Wang J, Pisani L, Caccia C, Carotti A, Salvati P, et al. Structures of human monoamine oxidase B complexes with selective noncovalent inhibitors: safinamide and coumarin analogs. J Med Chem. 2007; 50: 5848–5852. PMID: 17915852

15. Hubálek F, Binda C, Khalil A, Li M, Mattevi A, Castagnoli N, et al. Demonstration of isoleucine 199 as a structural determinant for the selective inhibition of human monoamine oxidase B by specific reversible inhibitors. J Biol Chem. 2005; 280: 15761–15766. PMID: 15710600

16. Son SY, Ma J, Kondou Y, Yoshimura M, Yamashita E, Tsukihara T. Structure of human monoamine oxidase A at 2.2-Å resolution: the control of opening the entry for substrates/inhibitors. Proc Natl Acad Sci USA. 2008; 105: 5739–5744. doi: 10.1073/pnas.0710626105 PMID: 18391214

17. Binda C, Li M, Hubálek F, Restelli N, Edmondson DE, Mattevi A. Insights into the mode of inhibition of human mitochondrial monoamine oxidase B from high-resolution crystal structures. Proc Natl Acad Sci USA. 2003; 100: 9750–9755. PMID: 12913124

18. Milczek EM, Binda C, Rovida S, Mattevi A, Edmondson DE. The 'gating' residues Ile199 and Tyr326 in human monoamine oxidase B function in substrate and inhibitor recognition. FEBS Journal. 2011; 278: 4860–4869. doi: 10.1111/j.1742-4658.2011.08386.x PMID: 21978362

19. Binda C, Aldeco M, Mattevi A, Edmondson DE. Interactions of monoamine oxidases with the antiepileptic drug zonisamide: specificity of inhibition and structure of the human monoamine oxidase B complex. J Med Chem. 2010; 54: 909–912. doi: 10.1021/jm101359c PMID: 21175212

20. Esteban G, Allan J, Samadi A, Mattevi A, Unzeta M, Marco-Contelles J, et al. Kinetic and structural analysis of the irreversible inhibition of human monoamine oxidases by ASS234, a multi-target compound designed for use in Alzheimer's disease. BBA-Proteins Proteom. 2014; 1844: 1104–1110.

21. Li M, Binda C, Mattevi A, Edmondson DE. Functional role of the "aromatic cage" in human monoamine oxidase B: structures and catalytic properties of Tyr435 mutant proteins. Biochemistry. 2006; 45: 4775–4784. PMID: 16605246

22. Bonivento D, Milczek EM, McDonald GR, Binda C, Holt A, Edmondson DE, et al. Potentiation of ligand binding through cooperative effects in monoamine oxidase B. J Biol Chem. 2010; 285: 36849–36856. doi: 10.1074/jbc.M110.169482 PMID: 20855894

23. Zapata-Torres G, Fierro A, Barriga-González G, Salgado JC, Celis-Barros C. Revealing Monoamine Oxidase B Catalytic Mechanisms by Means of the Quantum Chemical Cluster Approach. J Chem Inf Mod. 2015; 55: 1349–1360.

24. Atalay VE, Erdem SS. A comparative computational investigation on the proton and hydride transfer mechanism of monoamine oxidase using model molecules. Comput Biol Chem. 2013; 47: 181–191 doi: 10.1016/j.compbiolchem.2013.08.007 PMID: 24121676

25. Repic M, Vianello R, Purg M, Duarte F, Bauer P, Kamerlin SCL, et al. Empirical valence bond simulations of the hydride transfer step in the monoamine oxidase B catalyzed metabolism of dopamine. Proteins: Struct Funct Bioinf. 2014, 82:3347–3355

26. Abad E, Zenn RK, Kästner J. Reaction Mechanism of Monoamine Oxidase from QM/MM Calculations, J Phys Chem B, 2013, 117:14238–14246 doi: 10.1021/jp4061522 PMID: 24164690

27. Geha RM, Chen K, Wouters J, Ooms F, Shih JC. Analysis of conserved active site residues in mono-amine oxidase A and B and their three-dimensional molecular modeling. J Biol Chem. 2002; 277: 17209–17216. PMID: 11861643

28. Binda C, Mattevi A, Edmondson DE. Structural properties of human monoamine oxidases A and B. Int Rev Neurobiol. 2011; 100: 1–11. doi: 10.1016/B978-0-12-386467-3.00001-7 PMID: 21971000

29. Kalgutkar AS, Dalvie DK, Castagnoli N, Taylor TJ. Interactions of nitrogen-containing xenobiotics with monoamine oxidase (MAO) isozymes A and B: SAR studies on MAO substrates and inhibitors. Chem Res Toxicol. 2001; 14: 1139–1162. PMID: 11559028

30. Kinemuchi H, Arai Y, Toyoshima Y, Tadano T, Kisara K. Studies on 5-fluoro-α-methyltryptamine and p-chloro-β-methylphenethylamine: Determination of the MAO-A or MAO-B selective inhibition in vitro. JPN J Pharmacol. 1988; 46: 197–199. PMID: 3379831

31. Kim SK, Toyoshima Y, Arai Y, Kinemuchi H, Tadano T, Oyama K, et al. Inhibition of monoamine oxi-dase by two substrate-analogues, with different preferences for 5-hydroxytryptamine neurons. Neuro-pharmacology. 1991; 30: 329–335. PMID: 1852266

32. Newton-Vinson P, Hubálek F, Edmondson DE. High-level expression of human liver monoamine oxi-dase B in *Pichia pastoris*. Protein Express Purif. 2000; 20: 334–345.

33. Cossi M, Rega N, Scalmani G, Barone V. Energies, structures, and electronic properties of molecules in solution with the C-PCM solvation model. J Comput Chem. 2003; 24: 669–681. PMID: 12666158

34. Barone V, Cossi M. Quantum calculation of molecular energies and energy gradients in solution by a conductor solvent model. J Phys Chem A. 1998; 102: 1995–2001.

35. Siegbahn PE, Himo F. Recent developments of the quantum chemical cluster approach for modeling enzyme reactions. J Biol Inorg Chem. 2009; 14: 643–651. doi: 10.1007/s00775-009-0511-y PMID: 19437047

36. Ross GA, Morris GM, Biggin PC. Rapid and accurate prediction and scoring of water molecules in pro-tein binding sites. PLoS One. 2012; 7:e32036. doi: 10.1371/journal.pone.0032036 PMID: 22396746

37. Zhao Y, Truhlar DG. The M06 suite of density functionals for main group thermochemistry, thermo-chemical kinetics, noncovalent interactions, excited states, and transition elements: two new func-tionals and systematic testing of four M06-class functionals and 12 other functionals. Theor Chem Acc. 2008; 120: 215–241.

38. Gaussian 09, Revision E.01, Frisch MJ, Trucks GW, Schlegel HB, Scuseria GE, Robb MA, Cheeseman JR, et al. Gaussian, Inc., Wallingford CT, 2009.

39. Anslyn EV, Dougherty DA. Modern physical organic chemistry. Eds.; University Science Books: United States, 2006.

40. Contreras-García J, Johnson ER, Keinan S, Chaudret R, Piquemal JP, Beratan DN, et al. NCIPLOT: a program for plotting noncovalent interaction regions. J Chem Theory Comput. 2011; 7: 625–632 PMID: 21516178

41. Johnson ER, Keinan S, Mori-Sanchez P, Contreras-Garcia J, Cohen AJ, Yang W. Revealing noncova-lent interactions. Journal of the American Chemical Society, 132(18), 6498–6506. J Am Chem Soc. 2010; 13: 6498–6506 doi: 10.1021/ja100936w PMID: 20394428

42. Contreras-García J, Yang W. Analysis of hydrogen-bond interaction potentials from the electron den-sity: Integration of NCI regions J Phys Chem A, 2011, 115:12983–12990 doi: 10.1021/jp204278k PMID: 21786796

43. Heuson E, Storgaard M, Huynh TH, Charmantray F, Gefflaut T, Bunch L. Profiling substrate specificity of two series of phenethylamine analogs at monoamine oxidase A and B. Org Biomol Chem. 2014; 12:8689–8695 doi: 10.1039/c4ob01377h PMID: 25253656

44. Liao RZ. Quantum Chemical Cluster Modeling of Enzymatic Reactions. Ph.D. Thesis, Stockholm Uni-versity, Stockholm, Sweden, 2010. Available: https://www.diva-portal.org/smash/get/diva2:353152/FULLTEXT01.pdf

45. Celis-Barros C, Saavedra-Rivas L, Salgado JC, Cassels BK, Zapata-Torres G. Molecular dynamics simulation of halogen bonding mimics experimental data for cathepsin L inhibition. J Comp Aided Mol Des. 2015; 29: 37–46.

46. Edmondson DE, Bhattacharrya AK, Xu J. Evidence for alternative binding modes in the interaction of benzylamine analogues with bovine liver monoamine oxidase B. BBA Protein Struct Mol Enzym. 2000; 1479:52–58.